White Rose Research Online

eprints@whiterose.ac.uk
https://eprints.whiterose.ac.uk
Universities of Leeds, Sheffield and York

Deposited via The University of Sheffield.

White Rose Research Online URL for this paper:
https://eprints.whiterose.ac.uk/id/eprint/247196/

Version: Published Version

Article:
Ormiston-Lee, L.M., Furmidge, R., Workman, V.L. et al. (2026) Development and in vitro assessment of novel decellularised adipose sheets for adipose tissue regeneration. European Cells & Materials, 59. pp. 108-123. ISSN: 1473-2262

https://doi.org/10.22203/ecm.v059a07

Reuse
This article is distributed under the terms of the Creative Commons Attribution (CC BY) licence. This licence allows you to distribute, remix, tweak, and build upon the work, even commercially, as long as you credit the authors for the original work. More information and the full terms of the licence here: https://creativecommons.org/licenses/

Takedown
If you consider content in White Rose Research Online to be in breach of UK law, please notify us by emailing eprints@whiterose.ac.uk including the URL of the record and the reason for the withdrawal request.

UNIVERSITY OF LEEDS
University of Sheffield
UNIVERSITY of York

European Cells and Materials Vol.59 2026 (pages 108–123) DOI: 10.22203/eCM.v059a07 ISSN 1473-2262

Original Article

Development and *in vitro* Assessment of Novel Decellularised Adipose Sheets for Adipose Tissue Regeneration

Lucy M. Ormiston-Lee[1,2], Rachel Furmidge[3,4], Victoria L. Workman[3], Claire L. Brockett[4,5], Jennifer H. Edwards[1,2], Vanessa L. Hearnden[3,4,*] and Helen E. Berry[1,2,*]

[1]School of Biomedical Sciences, Faculty of Biological Sciences, University of Leeds, LS2 9JT Leeds, UK
[2]Institute of Medical and Biological Engineering, University of Leeds, LS2 9JT Leeds, UK
[3]Department of Chemical, Material and Biological Engineering, University of Sheffield, S1 3JD Sheffield, UK
[4]INSIGNEO Institute, University of Sheffield, S1 3JD Sheffield, UK
[5]Department of Mechanical Engineering, University of Sheffield, S1 3JD Sheffield, UK

Abstract

Background: Decellularised adipose tissue (DAT) is a potential regenerative treatment for adipose tissue regeneration; however, decellularisation often involves methods that compromise the integrity of the extracellular matrix architecture. This study aimed to develop a protocol to produce a sheet form of porcine-derived DAT and to assess the cellular response to DAT. **Methods:** A novel method of producing DAT was assessed using histology and biochemical assays to confirm decellularisation. An extract cytotoxicity assay was used to detect whether DAT was cytotoxic towards 3T3 and L929 cells. Following this, the DAT was cultured with 3T3 and 3T3-L1 (pre-adipocyte) cell lines for 28 days. Cell metabolism, viability and differentiation potential were investigated using alamarBlue™, live/dead and BODIPY 493/503 staining. Finally, the angiogenic potential of DAT was assessed using a chick chorioallantoic membrane (CAM) assay. **Results:** DAT was successfully produced in sheet form (from n = 6 pigs) with 7.96% lipid (relative to native tissue), 0.047 μg/mg sodium dodecyl sulphate and 0.50 ng DNA/mg of tissue remaining. The DAT was demonstrated to be non-cytotoxic to both 3T3 and L929 cells, supporting the attachment and migration of 3T3 and 3T3-L1 cell lines *in vitro*. DAT also supported the accumulation of lipids within 3T3-L1 cells and the directional growth of blood vessels *ex ovo*. **Conclusions**: A suitable method for producing DAT has been developed, resulting in DAT sheets that are non-cytotoxic, cytocompatible, and have the potential to support adipogenic differentiation and angiogenesis *in vivo*.

Keywords: Decellularisation, adipose tissue, regenerative materials.

***Address for correspondence**: Helen E. Berry, School of Biomedical Sciences, Faculty of Biological Sciences, University of Leeds, LS2 9JT Leeds, UK; Institute of Medical and Biological Engineering, University of Leeds, LS2 9JT Leeds, UK. E-mail: h.e.berry@leeds.ac.uk; Vanessa L. Hearnden, Department of Chemical, Material and Biological Engineering, University of Sheffield, S1 3JD Sheffield, UK; INSIGNEO institute, University of Sheffield, S1 3JD Sheffield, UK. E-mail: v.hearnden@sheffield.ac.uk.

Copyright policy: © 2026 The Author(s). Published by Forum Multimedia Publishing, LLC. This article is distributed in accordance with Creative Commons Attribution Licence (http://creativecommons.org/licenses/by/4.0/).

Introduction

Adipose tissue has important metabolic and mechanical functions that are crucial for the proper functioning of the body. White adipose tissue acts as an energy store that can be mobilised to release glucose to meet energy demand [1]. Alongside this, adipose tissue has essential functions in wound healing, including regulating macrophage function [2]. The large content of endogenous adipose-derived stromal cells (ADSCs) within adipose tissue promotes macrophage polarisation towards the M2 "repair" phenotype during normal wound healing [3,4].

Mechanically, adipose tissue acts as a shock-absorbent cushion to protect internal organs and bones from mechanical injury [5]. Where adipose tissue is lost as a result of trauma, resection or disease, it is crucial to regenerate adipose tissue deposits to restore these functions. Alongside this, cosmetic issues due to adipose tissue defects can significantly impact patients' mental health. The current 'gold standard' treatment for adipose regeneration is autologous fat transfer. Autologous fat transfer involves the removal of the patient's own fat from another area, often the abdomen, using liposuction, which is then injected into the site of the adipose tissue defect [6]. Although autologous fat transfer has demonstrated good clinical outcomes for volume restoration and scar revision, resorption of the implanted fat is a problem [6–9].

Another method being explored for regenerating adipose tissue is the use of ADSCs [10]. ADSCs can be implanted into the defect site with the expectation that they will grow, differentiate and regenerate the area. ADSC therapies have been shown to aid in the regeneration of various tissues, including cartilage and myocardium, through the differentiation into tissue-specific cells such as chondrocytes and cardiomyocytes, as well as promoting extracellular matrix (ECM) deposition [10–12]. The ADSCs have also been observed to promote angiogenesis via the release of proangiogenic factors, such as vascular endothelial growth factor [10]. As with all cell therapies, the need to isolate and grow autologous cells from fresh lipoaspirate means these therapies are expensive, time-consuming and logistically challenging [13]. Therefore, there is a need to develop alternative, effective, readily available, and safe methods for the regeneration of adipose tissue.

Decellularised tissues are a relatively recent development in the field of tissue engineering. Current clinical uses of decellularised tissues include decellularised dermis to treat skin injuries and decellularised heart valves for heart valve replacement [14,15]. The most widely used decellularised tissue is decellularised small intestinal submucosa, which has been approved for many uses, such as wound dressings and hernia repairs [16,17]. The production of decellularised tissues involves the removal of the cells to leave behind the ECM, which acts as a framework for the migration of the patient's cells into the site of implantation [18]. Removing the cellular contents of the tissue removes the immunogenic material, significantly reducing the likelihood of evoking an adverse immune response. The remaining ECM plays a crucial role in cell adhesion, cell signalling, restoration of tissue architecture and structural stability [19–21]. In wound healing, the ECM modulates cell behaviour via biochemical and biomechanical pathways. For example, it is the initial deposition of fibronectin network in granulation tissue that produces a scaffold for the formation of a vascularised network that, in turn, supports collagen deposition [22,23].

Producing decellularised tissues from adipose tissue has the potential to generate ECM which has the required biochemical and biomechanical cues for adipose tissue regeneration. Decellularised adipose tissue (DAT) can be stored long-term and does not need to be donor-matched, meaning DAT has the potential to be an "off-the-shelf" treatment [24,25]. Within literature, DAT has been derived from various sources, including rat, porcine, and human adipose tissue [26–28]. It has been widely investigated both *in vitro* and *in vivo* for its potential as an adipose regenerative material [9,19,29]. Preclinical studies have demonstrated that DAT can be repopulated with ADSCs *in vitro* [19] and produce promising outcomes in mouse models [29]. Human-derived DAT has also been tested in a Phase I clinical trial to look at volume retention compared to autologous fat grafting. Anderson *et al*. [30] (2022) demonstrated that a human-derived DAT could produce comparable volume retention compared to autologous fat grafting 18 weeks after abdominal injection into 8 healthy participants but unlike autologous fat grafting, there was no evidence of cysts or calcification. The implanted DAT grafts were shown to support cellular infiltration and pro-regenerative T cell and macrophage phenotypes [30].

Previous examples of DAT production have processed tissue in ways which disrupt the ECM arrangement, including freeze-thaw cycles and mechanical massaging [25,31]. Producing decellularised materials in sheet form, which preserves more of the ECM arrangement and structure has been described as useful for soft tissue and cardiac repair [32]. Our hypothesis is that DAT in sheet form will be more beneficial to maintain ECM molecule interactions and organisation after implantation [33]. Previously, ADSC cell sheets have been utilised to improve the healing of full-thickness dermal wounds and the sheet form enabled the production of 3D structures by layering the sheets [34]. One of the challenges of cell derived sheets is their fragility and their ability to be handled [35], however decellularised tissue sheets have the potential to be produced in a way which maintains the endogenous tissue strength and integrity and increases their suitability for certain clinical applications, such as diabetic foot ulcers and breast reconstruction, which require structural support and surgical implantation.

This project aimed to produce porcine-derived DAT sheets that met the criteria for effective decellularisation and to test their biocompatibility. The decellularisation criteria were: residual double stranded DNA (dsDNA) levels below 50 ng/mg [36], > 90% lipid removal, and a residual detergent below cytotoxic levels *in vitro*, which has previously been reported as 10 µg/mg of tissue [37]. The resulting DAT was tested for its ability to support adhesion, growth and proliferation of fibroblast (3T3) and adipocyte-like (3T3-L1) cell lines *in vitro* and the growth of new blood vessels in the chick chorioallantoic membrane (CAM) assay *ex ovo*. This approach was used to indicate whether DAT is likely to support cell growth and vascularisation *in vivo*, therefore aiding healing and integration of the DAT.

Materials and Methods

Decellularisation

Samples of subcutaneous adipose tissue from six Large White pigs were dissected using a dermatome (Padgett, Integra, UK, Model B) to produce thin sheets of adipose tissue (~1–2 mm thick, 4 cm^2 area). Two sheets were then placed into a 250 mL sealed bioprocess bag (Thermo Fisher Scientific, UK, SS00003I) for each animal. The solution changes in the decellularisation process were carried out aseptically in a Class II biological safety cabinet. For all steps, 200 mL of solution was used, except for the Nuclease solution, for which 80 mL was used. All steps were carried out at 42 °C with horizontal agitation at 220 rpm, except the nuclease solution steps, which were carried out

at 37 °C and 80 rpm.

Samples were washed with hypotonic buffer (10 mM Tris (Sigma Aldrich, UK, 1003399030), 2.7 mM Ethylenediaminetetraacetic acid (EDTA) (Thermo Fisher Scientific, UK, E/P140/53), 10 KIU/mL aprotinin (Nordic, UK, 08718481142905)) for 1 hour. Following this, samples were washed with IPA-SDS solution [70% (v/v) isopropanol (IPA) (Thermo Fisher Scientific, UK, P/7490/21) and 30% sodium dodecyl sulphate (SDS) hypotonic buffer (0.1% w/v SDS (Sigma Aldrich, UK, 71725), 10 mM Tris, 2.7 mM EDTA, 10 KIU/mL aprotinin) resulting in a final working concentration of 0.03% SDS in IPA-SDS solution] for 1 hour, this was then replaced with fresh IPA-SDS solution and washed for a further 30 minutes. Then two sequences of 1 hour in 100% IPA and 30 minutes in 70% IPA were undertaken, followed by a further 1 hour in 100% IPA. Following this, the IPA was replaced with fresh 100% IPA and left overnight (∼17 hours). The following day, two 30-minute IPA-SDS solution washes, one 2-hour 100% IPA wash and one 3-hour IPA-SDS solution wash were undertaken in that order. This was then replaced with SDS hypotonic buffer, and the tissues were washed for 70 minutes. This was replaced with phosphate buffered saline (PBS) (Oxoid, UK, BR0014G) containing aprotinin (10 KIU/mL) and left overnight (∼17 hours). The following day, three 15-minute PBS washes were undertaken for the removal of chemicals and aprotinin before nuclease addition. Then the PBS was replaced with 80 mL of Nuclease solution (50 mM Tris, 1 mM $MgCl_2$(VWR, UK, 7786-30-3), 10 U/mL Benzonase (Novagen, UK, 71205-3)) and washed for 1 hour, carried out at 37 °C and 80 rpm. This was replaced with fresh nuclease solution and repeated a second time. Following this, the tissues were washed with PBS again for a further three 15-minute washes. Then the PBS was replaced with hypertonic buffer (50 mM Tris, 1.5 M NaCl (Thermo Fisher Scientific, UK, S/3160/63)) for 1 hour. Following this, the tissue was washed with a hypotonic buffer without aprotinin (10 mM Tris, 2.7 mM EDTA) for 1 hour, and then again with a hypertonic buffer for a further hour. Finally, a further three 15-minute PBS washes were carried out to remove any residual detergent.

Histology & Microscopy

Samples of DAT and native adipose tissue (NAT) were fixed in 10% neutral buffered formalin (NBF) (Atom Scientific, UK, RRFF4000-G) for ∼12 hours, processed and then embedded in paraffin wax (Epredia, UK, 6774060). Sections were cut at 8 μm thickness, dewaxed using xylene (VWR, UK, 28975.360), and then rehydrated before staining. 4′,6-diamidino-2-phenylindole (DAPI) staining (1 mg/mL) (Merk Millipore, UK, 10236276001) was used to verify decellularisation, and viewed using a DAPI filter at 335–383 nm, 420–470 nm (excitation range, emission range) with a Zeiss upright light microscope (Zeiss, UK, AXIO imager.M2). Mayer's Haematoxylin (Atom Scientific, UK, RRSP60-E) and eosin Y (Sigma Aldrich, UK, 1.09844.1000) (H&E) staining was used to visualise the tissue structure, including cell nuclei and ECM.

DNA Quantification

Both NAT (20 mg) and DAT (100 mg) were macerated and lyophilised to a constant weight in a ModulyoD-230 freeze-drier (ThermoSavant, UK, ModulyoD-230). DNA was extracted using a DNeasy kit (Qiagen, UK, 69506) following the manufacturer's instructions. After DNA was extracted, it was quantified using a Quant-iT^{TM} PicoGreen^{TM} assay (Thermo Fisher Scientific, UK, P7589), and the results were normalised to the lyophilised tissue mass of the sample.

Lipid Quantification

Lipid quantification was adapted from a previous study [38]. Lipids were extracted from NAT (20 mg) and DAT (100 mg) via incubation in 5 mL absolute ethanol for 72 hours at 42 °C with gentle agitation (120 rpm). The lipid-containing ethanol was diluted in a 1:6 ratio to produce 600 μL of each sample and 100 μL of 2 M hydroxylamine hydrochloride (Sigma Aldrich, UK, 5470-11-1) solution and 100 μL of 3.5 M sodium hydroxide (Thermo Fisher Scientific, UK, S/4920/60) solution were added to all test samples and lipid standards (Concentration range 0 μg/mL – 2500 μg/mL, 600 μL volumes) and left to incubate for 20 minutes at room temperature. Following this, 100 μL of 4 M hydrochloric acid solution (VWR, UK, 2611.5000) and 100 μL of 0.37 M iron (III) chloride solution (Sigma Aldrich, UK, 10025-77-1) were added to all samples and standards and absorbance was measured at 540 nm. Sample concentrations were extrapolated from standards and data were normalised to sample mass before assay to provide μg of lipid per mg of tissue mass. Mass loss during freeze-drying was then used to calculate μg of lipid per mg lyophilised tissue.

Sodium Dodecyl Sulphate Quantification

Residual SDS was extracted from DAT (100mg) via incubation at 37 °C in 1 mL distilled water with gentle agitation for 72 hours. Stains-All working solution [50 μg/mL Stains all (Sigma Aldrich, UK, E9379), 5% formamide (Honeywell, UK, F7503), 2.5% IPA] was added to each standard and sample, and the absorbance was measured at 447 nm. Sample concentrations were extrapolated from SDS standards of concentrations ranging between 0 μg/mL and 200 μg/mL and then normalised to tissue mass.

Cell Culture

3T3 mouse fibroblastic cells (3T3 Swiss Albino, ECACC # 85022108; purchased from UK Health Security Agency [UKHSA], Salisbury, UK) and 3T3-L1 mouse fibroblast cells (ATCC # CL-173; purchased from LGC, Middlesex, UK) were grown in complete growth medium

[Dulbecco's Modified Eagles Medium (DMEM) (Corning, UK, 90-013-PB) supplemented with 10% heat-inactivated foetal bovine serum (FBS) (Sigma Aldrich, UK, F9665), 100 U/100 μg/mL Penicillin/Streptomycin (Merk Millipore, UK, P4458) and 4 mM L-Glutamine (Merk Millipore, UK, G7513)] and L929 mouse fibroblastic cells (ECACC # 85011425; purchased from UKHSA, Salisbury, UK) were grown in L929 complete growth medium (DMEM supplemented with 10% FBS, 100 U/100 μg/mL Penicillin/Streptomycin and 2 mM L-Glutamine) unless otherwise stated. Cells were grown at 37 °C in a humidified incubator with a 5% CO_2 supply and passaged every 2-3 days during maintenance and expansion. The purchased cell lines were certified as mycoplasma-free (PCR). 3T3 cells were chosen to investigate fibroblast cytocompatibility; 3T3-L1 cells were chosen to investigate adipocyte cytocompatibility, and L929 cells were chosen as a cell line of interest based on the examples provided within the standard for cytotoxicity testing (ISO 10993:5, 2018).

Sterility

Sterility was tested by incubation at 37 °C in a thioglycolate medium USP broth (50 mL; Oxoid, UK, CM0173) for 2 weeks and compared to negative (sterile broth) and positive (floor swab) controls of microbial growth at 2 days, 1 week and 2-week time points.

Extract Cytotoxicity

Based on the ISO 10993-5 standard for cytotoxicity testing of biomaterials guidelines, DAT samples were macerated and incubated in DMEM at a ratio of 100 mg tissue:1 mL DMEM for 72 hours at 37 °C with continuous agitation to produce DAT extract media (ISO 10993-5, 2018). Cells were seeded onto a 96-well plate at a density of 7.81 $\times$ 10^4 cells/cm^2, 200 μL volume for both L929 and 3T3s and allowed to attach for 24 hours. Growth of cells with neat DAT extracts was compared to positive control media (DMEM containing 40% Dimethylsulphoxide [DMSO; Sigma Aldrich, UK, D2650] or negative control media (supplemented DMEM only). Cell morphology was observed using phase contrast microscopy. The metabolic activity of the cells was determined using an ATP-Lite assay (Perkin Elmer, UK, 6016947), according to the manufacturer's instructions.

Decellularised Adipose Tissue Seeding

DAT samples were cut using an 8 mm biopsy punch (Acuderm, Florida, United States, P810) and placed into an uncoated 48-well plate (CytoOne, Starlab, UK, CC7672-7548). DAT were seeded at a density of 5.3 $\times$ 10^5 3T3 cells/mm^3 in 20 μL of complete DMEM, which was placed on top of the DAT and then incubated at 37 °C with a 5% CO_2 supply for at least 2 hours before adding 500 μL of additional media. The media was changed every 2 days throughout the culture. The same method was followed with 3T3-L1 cells; however, these were seeded with 3.07 $\times$ 10^5 cells/mm^3 due to the larger size of the 3T3-L1 cells. Both 2D-cell-only and DAT-only controls were seeded at the same density within the appropriate experiment to ensure comparability.

After seeding, the DAT was fixed and processed as previously stated. Sections of DAT were collected from approximately 250 μm below the cell-seeded surface and stained with H&E to identify cell migration into the scaffold over time. These were imaged as previously stated.

Measurement of Metabolic Activity

alamarBlue™ (Bio-Rad, UK, BUF012B) was used to measure 3T3 and 3T3-L1 cell metabolic activity when grown in DAT compared to cell culture plastic. alamarBlue™ was added to the cells at 10% dilution in complete growth medium (as described in cell culture; Materials and Methods), and incubated for 3 hours. The percentage reduction of alamarBlue™ was used as an estimate for cell viability to indicate whether the cells remained alive throughout culture, calculated using the manufacturer's instructions.

Cell Staining

Live-dead staining (Invitrogen, Thermo Fisher Scientific, UK, L3224) of whole scaffolds was performed with Calcein AM (1 μM) and Ethidium homodimer-1 (1 μM). Stained DAT were imaged on a Zeiss LSM880 and Airyscan Inverted Confocal Microscope (Zeiss, UK, LSM880) at 488 nm, 537 nm (excitation, emission) and 561 nm, 661 nm (excitation, emission) wavelengths, respectively. BODIPY 493/503 neutral lipid stain (5 μM) (Cambridge Bioscience, UK, 25892) and DAPI (2.86 mM) were used to visualise lipid accumulation. 3T3-L1 cells on the DAT were incubated for 30 minutes with the stains prior to imaging. BODIPY 493/503 and DAPI were imaged at 488 nm, 538 nm (excitation, emission) and 405 nm, 442 nm (excitation, emission) wavelengths, respectively.

Vascularisation Analysis

A CAM assay study was carried out to assess whether the DAT was capable of supporting directional vessel growth *ex ovo*, as previously described [39]. Fertilised Shaver Brown chicken eggs (Medeggs Ltd, UK, no product code) were incubated at 37.5 °C in an Ova-Easy Series II Advanced Cabinet Incubator with 45% humidity produced by an Ova-Easy/TLC Advance Humidity Pump attachment (Brinsea, USA, MJ3823C). The embryos were removed from their shells and grown in curved weighing boats with 3 mL of PBS containing 1% Penicillin/Streptomycin (100 U/100 μg/mL) and 1% Amphotericin B (250 μg/mL) (Gibco, UK, 15290-026). Following this, the weighing boats were placed in petri-dishes containing 4 mL PBS and incubated in a humidified incubator at 38 °C with 0.05% CO_2 supply from day 3 of incubation [40]. On day 7 of

incubation, 10 mm diameter circles of DAT were added on top of the allantoic membrane and positioned so that they were in contact with the upper membrane. On day 13, white hand cream was injected under the upper membrane as a contrast agent. Then, DAT on the CAM were imaged using an UltraMZ-0460 Monozoom Industrial Inspection Microscope with a USB camera with GXCapture-T software (G. T. Vision, UK, UltraMZ-0460) and then analysed using Fiji ImageJ [41] to assess vessel density as well as directional vessel growth. The DAT and the adjacent layer of the CAM were fixed using 10% NBF and taken for histological analysis using H&E staining as described previously. For analysis, images were correctly scaled, cropped, converted to 3-bit images, and then sharpened. Following this, the directional growth of perpendicular (± 45°) vessels was measured as described in [39]. For vessel density, the images were then thresholded using the "Mexican hat" filter, despeckled and then analysed with the "Vessel analysis" plugin [42].

Data Analysis & Statistics

Where relevant, data were represented graphically and presented as the mean ± standard deviation. For image data, representative images were taken from the sample cohort. Image analysis was undertaken over 5 separate areas in at least 4 different images per condition using ImageJ. For measurements of cell diameter, this was taken across the largest part of the cell over 8 random areas within 6 different images per sample.

Statistical analysis was undertaken where appropriate and stated within the figure legend. Data were tested for normality using the Shapiro-Wilk or Kolmogorov-Smirnov test, and in the case that data were not normally distributed, the non-parametric test was undertaken. Where data is presented as proportional data and statistical analysis has been undertaken, data has been transformed to radians using the arcsine function to fit the data to a Gaussian distribution, allowing for statistical analysis with the appropriate test. Data are displayed graphically as original percentages (mean ± standard deviation), with statistical significance calculated from transformed data displayed as * on the graph.

Results

Decellularisation of Porcine Adipose Tissue

Porcine NAT sheets were decellularised and then assessed using histological and biochemical analyses. Following decellularisation, the DAT sheet remained intact, becoming a transparent white colour (Fig. 1**A–B**). Average sheet thickness reduced from 1.32 cm in NAT to 0.98 cm (n = 6) in DAT, causing a percentage loss of 25.8%. Though reduced in thickness, the DAT sheet was easy to handle, remained intact when lifting, and pulling pressure could be applied without tissue breakage.

Histological analysis demonstrated a lack of nuclei within both the DAPI (Fig. 1**E**) and H&E (Fig. 1**G**) images of DAT compared to native tissue (Fig. 1**D–F**). Some autofluorescence of the ECM can be seen in the DAPI-stained DAT (Fig. 1**E**). DNA quantification was carried out (Fig. 2A), which provided clarification that this is not residual nuclei. Fig. 1**G** shows that the ECM architecture was maintained in DAT. Shrinkage of the basement membrane, which previously surrounded the adipocytes, was observed (Fig. 1**F–G**). The mean diameter of basement membrane gaps was significantly greater in NAT compared to DAT (53 μm and 23 μm, respectively; Fig. 1**C**).

No microbial growth was seen for any of the DAT samples incubated in thioglycolate broth (data not shown).

Extractable dsDNA content in the DAT was reduced to 0.50 ng/mg (± 0.14 ng/mg) of lyophilised tissue compared to 114.5 ng/mg (± 28.3 ng/mg) lyophilised tissue seen in the NAT (Fig. 2**A**). Free lipid content was reduced from 1454 μg/mg (± 560.7 μg/mg) to 115.8 μg/mg (± 72.7 μg/mg) demonstrating that 92.04% of the lipids have been removed (Fig. 2**B**). Extractable SDS content was 0.047 μg/mg (± 0.021 μg/mg) of hydrated tissue in DAT.

Cytotoxicity of DAT to L929 and 3T3 Cells

DAT was shown to be non-cytotoxic to both cell lines; there was no difference in cell morphology in cells grown with DAT extract compared to the negative control (cells cultured without extract) (L929 Fig. 3**A–C**, 3T3 Fig. 3**D–F**). The ATP production was significantly greater for both cell lines in the negative control and DAT than in the positive control (40 % DMSO) (L929 Fig. 3**G**, 3T3 Fig. 3**H**).

3T3 Cell Adhesion and Migration to DAT

Serial sectioning of the DAT enabled assessment of 3T3 cell migration through the DAT. Transverse sections were taken ~250 μm from the external (seeded) surface at the midpoint of the sample after shrinkage during histological processing (Fig. 4) [43]. A greater number of cells (stained with purple haematoxylin) were visible at later time points, and the average number of cells per field of view increased from 0 at day 1 to 403 at day 28.

Cell Viability

Metabolic activity of 3T3 cells within DAT stayed consistent throughout the culture time. It was comparable to the cell-only control throughout, except for at days 14 and 21 (Fig. 5**A**), when metabolic activity was significantly greater in the 3T3 control. The live-dead staining at the end of the 28 days of culture showed that the majority of 3T3 cells were still alive, as mostly green cell staining was seen as opposed to the 3T3 cells grown with 40% DMSO, where the majority of cells were stained green (Fig. 5**B**). The proportion of live to dead cells was similar in the 3T3 control and DAT (Fig. 5**C**).

The 3T3-L1 cell viability remained consistent throughout 28 days of culture in DAT. This was comparable to that of the 3T3-L1 cell control at days 3 and 7, but

significantly lower than that of the 3T3-L1 cell control at the later time points (Fig. 6**A**). No metabolic activity was measured in the DAT only.

The majority of 3T3-L1 cells in DAT were alive after 28 days of culture, as they were stained green with live-dead, whereas 3T3-L1 cells grown with 40% DMSO were predominantly stained red (Fig. 6**B**). There was a similar proportion of live cells in the 3T3-L1 cells grown in DAT compared to the 3T3-L1 cells on tissue culture plastic (Fig. 6**C**).

Cell Differentiation

BODIPY 493/503 staining of 3T3-L1 cells shows the presence of neutral lipids in the DAT + 3T3-L1 cells after 28 days of cell culture in complete growth medium without the addition of chemical differentiation mediators (Fig. 7). A similar amount of lipids was observed in both 3T3-L1 cells grown in DAT and on tissue culture plastic. However, in both conditions, the lipid droplets in 3T3-L1 cells were smaller than those seen in adipocytes in NAT.

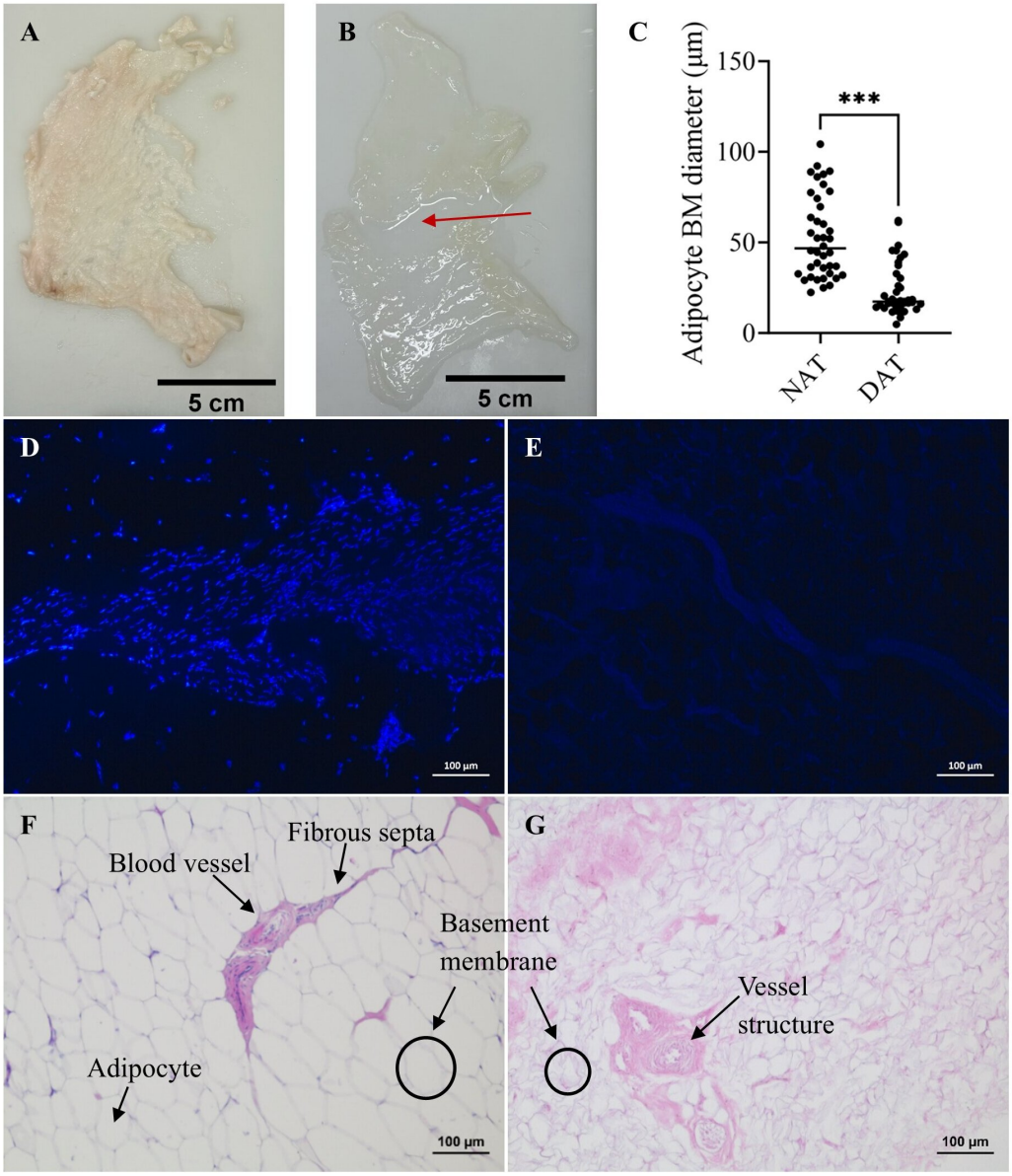

Fig. 1. NAT and DAT stained with DAPI and H&E. Representative images of native (**A,D,F**) and decellularised (**B,E,G**) porcine adipose tissue, imaged macroscopically (**A**, **B**, scale bar = 5 cm) (Red arrow highlights where the DAT had been cut to take samples for analysis), and microscopically (**D–G**, Scale bars = 100 μm) stained with DAPI (**D,E**) and H&E (**F,G**). Diameter of the basement membrane (BM) pockets which contained adipocytes were measured before and after decellularisation (**C**) (6 random areas were chosen per image across 6 images, one for each animal; n = 6, graphs showing median and the spread of the dataset), ***$p < 0.001$ analysed using unpaired two-tailed Student's *t*-test.

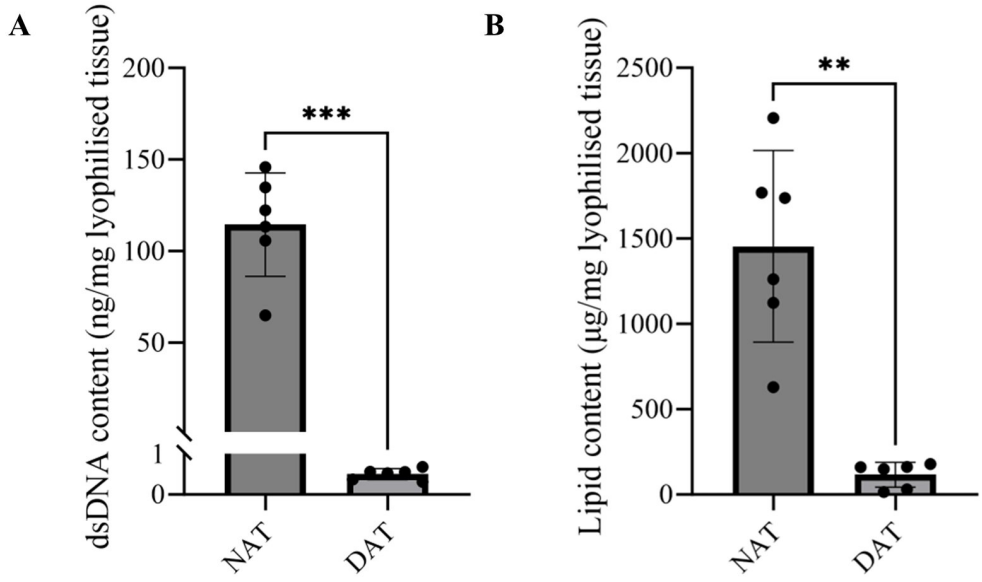

Fig. 2. DNA (A) and Lipid (B) content in native and decellularised adipose tissue. Total extracted DNA (**A**) and lipid (**B**) content from native and decellularised porcine adipose tissue (DAT) sample. Data is shown as mean ng DNA per mg of lyophilised tissue (**A**) and mean µg of lipid (**B**) per mg of lyophilised tissue (calculated by estimation based on an average mass loss of 12.3% in NAT and 86.8% of DAT after lyophilisation). (n = 6, mean ± standard deviation), $^{**}p < 0.002$, $^{***}p < 0.001$, analysed using a paired two-tailed Student's *t*-test (**A**) and a Mann-Whitney test (**B**).

Vascularisation

The ability of DAT to support vessel growth and cell infiltration in a CAM assay was assessed. A high survival rate of 66% was observed after the eggs were removed from cells. The images from the CAM assay show directional vessel growth towards the DAT, and vessel density greater than the control group (Fig. 8**A–C**, n = 6). An average of 33 (± 12) vessels grew directionally towards the DAT. This was significantly greater than the number of vessels that grew directionally towards the same circular area in the CAM only control, which were counted as an average of 19 (± 5) (Fig. 8**B**). Vessel density was also greater in DAT + CAM than in the control group, with a density of 14% (± 5%) area coverage by vessels in DAT + CAM compared to 9% (± 4%) area coverage by vessels in the CAM alone (Fig. 8**C**). H&E images of where the CAM and DAT were in contact highlight the close growth of vessels to DAT as well as cell infiltration from the CAM into DAT (Fig. 8**D–E**).

Discussion

This study demonstrated the successful production of DAT sheets with less than 1 ng of extractable dsDNA per mg of lyophilised DAT. This is well below the 50 ng/mg dsDNA outlined within previous literature as the level at which the material is expected not to evoke an adverse immune response [36]. We also demonstrated that extractable residual detergent levels (< 0.05 μg/mg, SDS) were ~200-fold lower than the cytotoxic level (10 μg/mg of tissue) stated in the literature [37], suggesting that the DAT would be safe for implantation with respect to detergent toxicity. This was also confirmed by the lack of cytotoxic responses in both *in vitro* and *ex ovo* models within the current study. Additionally, the resultant DAT sheet was easy to handle, demonstrating that DAT sheets maintained sufficient mechanical strength to be handled.

During the decellularisation process, a hypotonic buffer containing SDS and IPA was used to lyse the adipocytes and solubilise the intracellular lipids, respectively [31]. The use of 1% SDS in the decellularisation of anterior cruciate ligament allografts has previously been shown to damage ECM structure and integrity and inhibit cell migration [44]. However, in the current study, cells were viable after 28 days in culture and were able to migrate into the tissues effectively. Therefore, this suggests that the lower 0.01% SDS did not negatively impact cell growth or cause cytotoxicity within DAT, even though some alterations to the ECM were observed. The current study demonstrated that the decellularisation protocol resulted in a 92.04% reduction of lipids. This proportion of lipid removal appeared to be superior to previous methods involving lipases or ethanol, with these papers demonstrating remaining visible lipids in Oil Red O images [19,27,45]. However, none of these studies quantified the remaining lipids within DAT. Although there is no literature surrounding the optimal or "safe" levels of lipid within DAT, the removal of lipids during decellularisation remains impor-

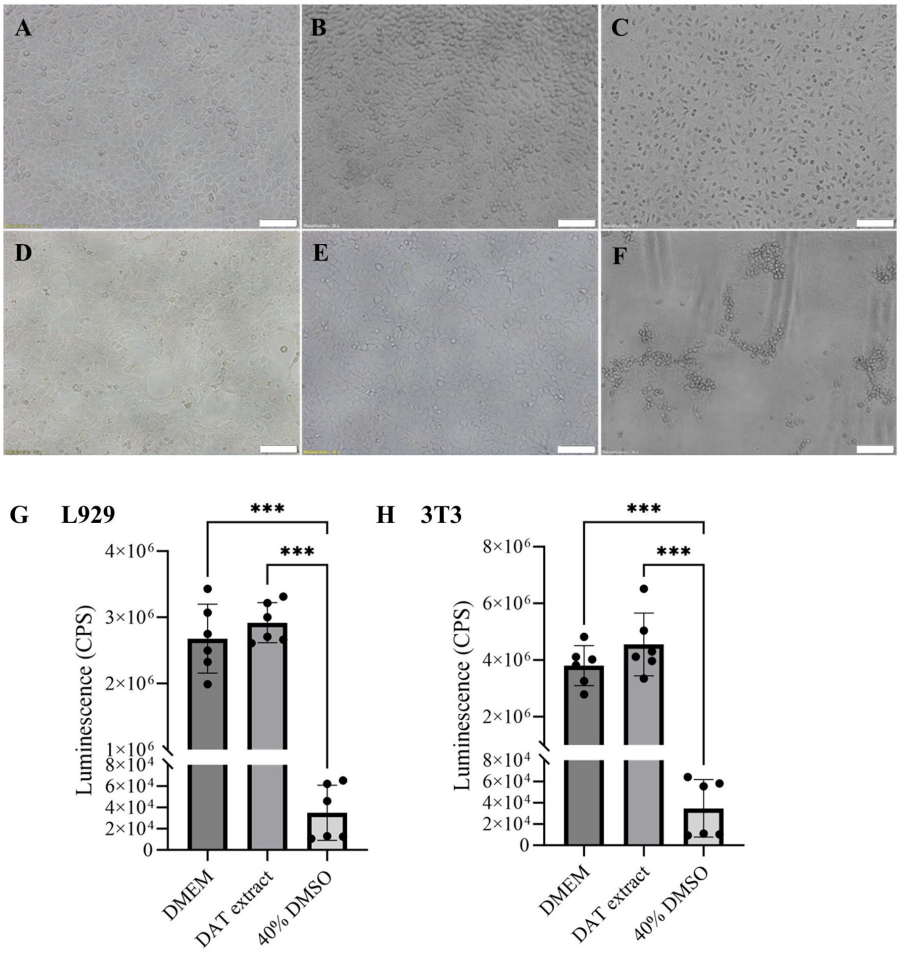

Fig. 3. DAT extract cytotoxicity on L929 and 3T3 cell lines. Representative images showing the cell morphology of L929 (**A–C**) and 3T3 (**D–F**) when grown in DAT extract media (**A** and **D**) compared to negative controls (DMEM) (**B** and **E**) and positive controls (40% DMSO) (**C** and **F**) (Scale bars = 100 μm). Brightness and contrast have been edited to better show cell morphology. The effect the extract had on the metabolism of L929 and 3T3 was measured using an ATP-Lite assay (**G** and **H**, respectively). (n = 6, mean ± standard deviation). ***$p < 0.001$, analysed using a Brown-Forsythe and Welch one-way ANOVA.

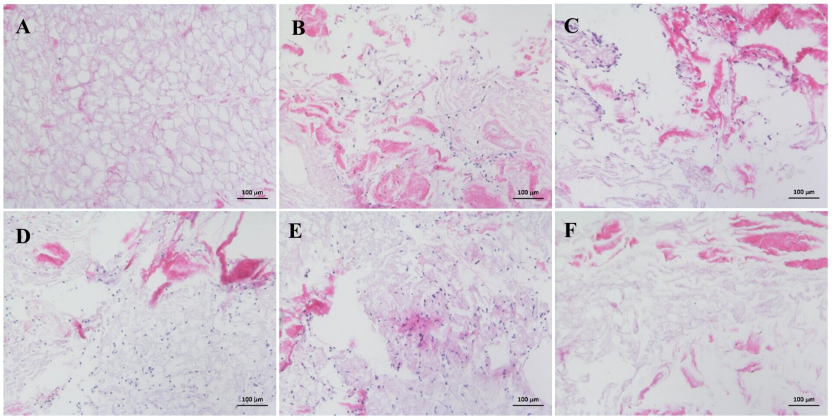

Fig. 4. Representative Haematoxylin and Eosin (H&E) stained images of DAT seeded with 3T3 cell line over 28 days. Central (~250 μm deep) sections of 3T3 seeded DAT stained with H&E grown for 1 day (**A**), 7 days (**B**), 14 days (**C**), 21 days (**D**), 28 days (**E**) compared to a scaffold only control (**F**). ECM stains pink and cell nuclei stain dark blue. Scale bars represent 100 μm.

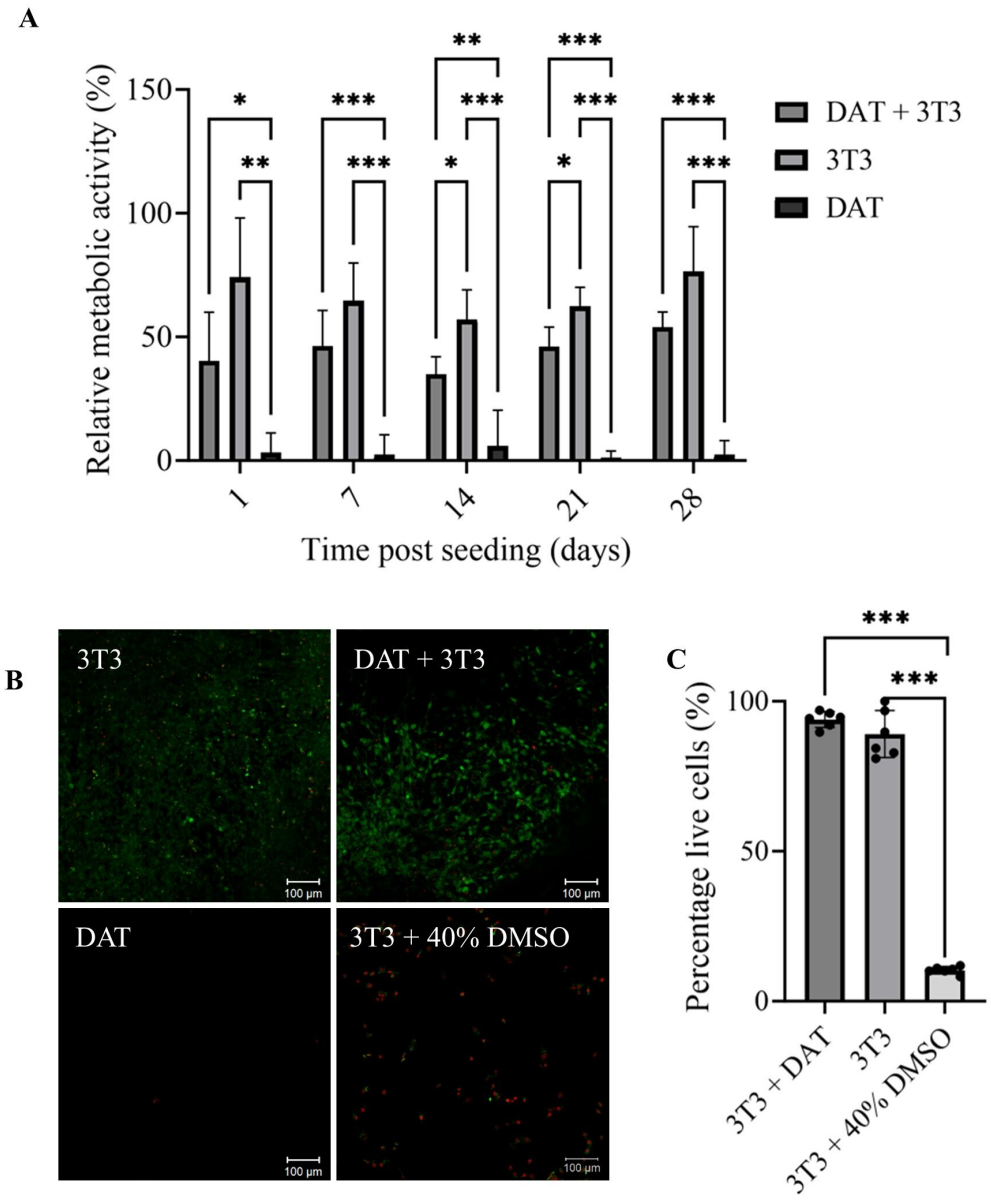

Fig. 5. 3T3 cell viability grown on DAT for 28 days compared to 3T3 or DAT only cells. 3T3 cell percentage viability measured with alamarBlue™ over 28 days of culture (**A**) 3T3 cells grown in DAT for 28 days compared to a 3T3, DAT and 3T3 + 40% DMSO controls stained with live/dead. Scale bars represent 100 μm. Live cells appear green and dead cells appear red (**B**) Graph shows the proportion of live cells in each condition, counts from Fiji, ImageJ (**C**) (n = 6, graphs show mean ± standard deviation). *$p < 0.033$, **$p < 0.002$, ***$p < 0.001$, assessed using arcsine data transformation and a two-way ANOVA with a Tukey's post-hoc test.

tant to reduce the risks associated with the presence of free lipids, such as fat emboli [46].

Sheet ECM has been produced from other materials, such as skin and small intestinal submucosa [47,48]. However, to the best of our knowledge, only one other study has described the production of adipose ECM sheets; these were produced from liposuction aspirate and then cast within a mould [49]. The maceration and recasting of the ECM in Kim *et al.* [49] (2012)'s protocol suggests that the original ECM architecture would have been damaged and redistributed during production, unlike the method in the present study. Although in this study, decellularisation resulted in a collapse of the basement membrane, the basement membrane could still be distinguished from the fibrous septa. A similar collapse of the basement membrane was shown in histological images in a decellularised human adipose tissue produced in a previous study, though the authors did not state this collapse [27]. Wang *et al.* [27] (2013) showed successful cell infiltration, ECM remodelling and growth of vasculature within the scaffold *in vivo*;

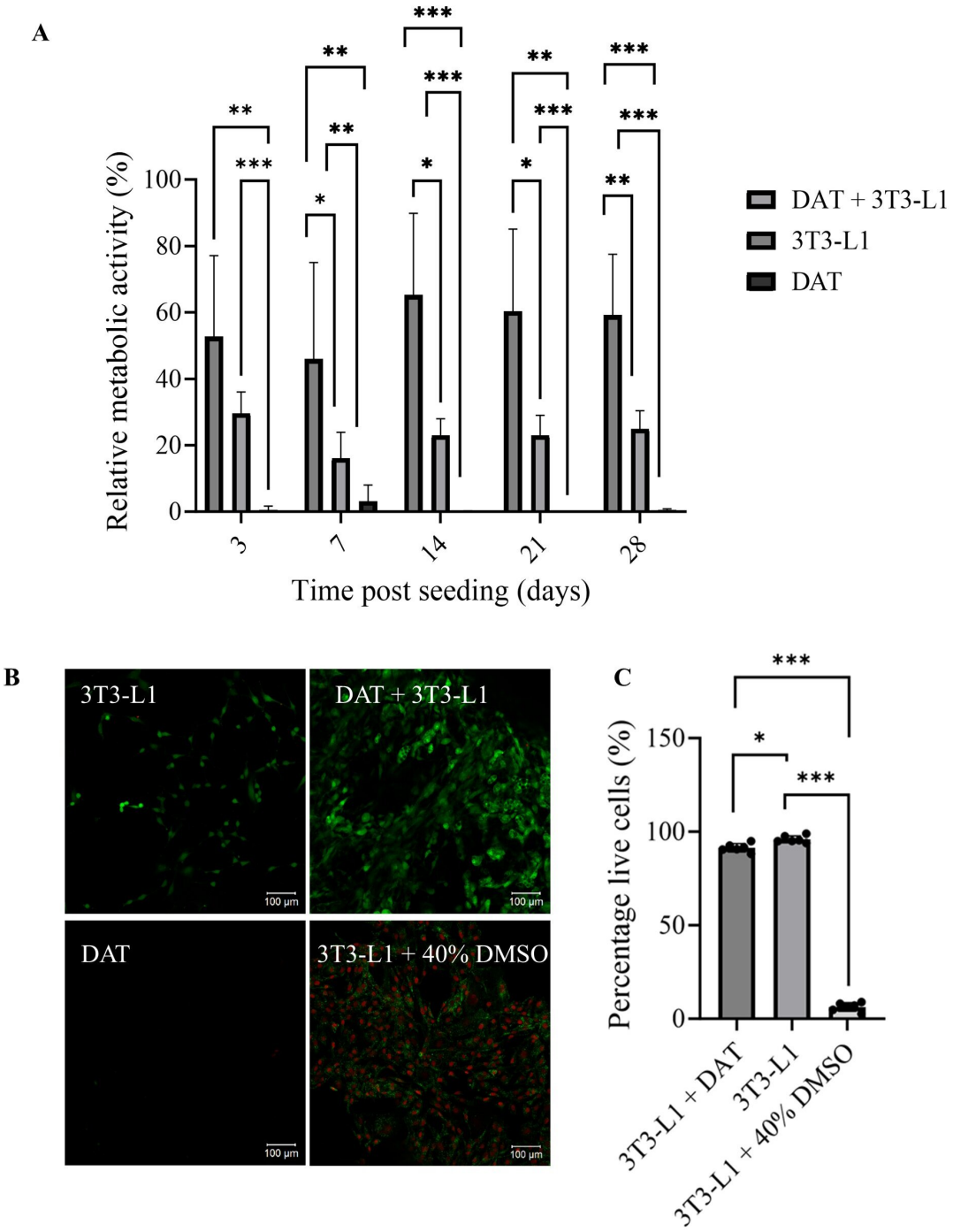

Fig. 6. 3T3-L1 cell viability grown on DAT for 4 weeks compared to 3T3-L1 and DAT only controls. 3T3-L1 cell % viability measured with alamarBlue™ over 4 weeks of culture (**A**) 3T3-L1 cells grown in DAT for 4 weeks compared to a 3T3-L1, DAT and 3T3-L1 + 40% DMSO controls stained with live/dead (**B**) Scale bars represent 100 μm. Live cells appear green and dead cells appear red. Graph shows the proportion of live cells in each condition, counts from Fiji, ImageJ (**C**) (n = 6, mean ± standard deviation). *$p <$ 0.033, **$p < 0.002$, ***$p < 0.001$, assessed using arcsine data transformation and a two-way ANOVA with a Tukey's post-hoc test.

therefore, this collapse is unlikely to cause a negative impact on DAT integration *in vivo*. Even so, more of the structure of the DAT produced in this study was maintained in comparison to other protocols, which involved maceration or digestion of the tissue pre- or post-decellularisation for DAT production or an ECM hydrogel [25,31]. For example, more of the basement membrane can be distinguished in H&E images of DAT in the current study, suggesting that

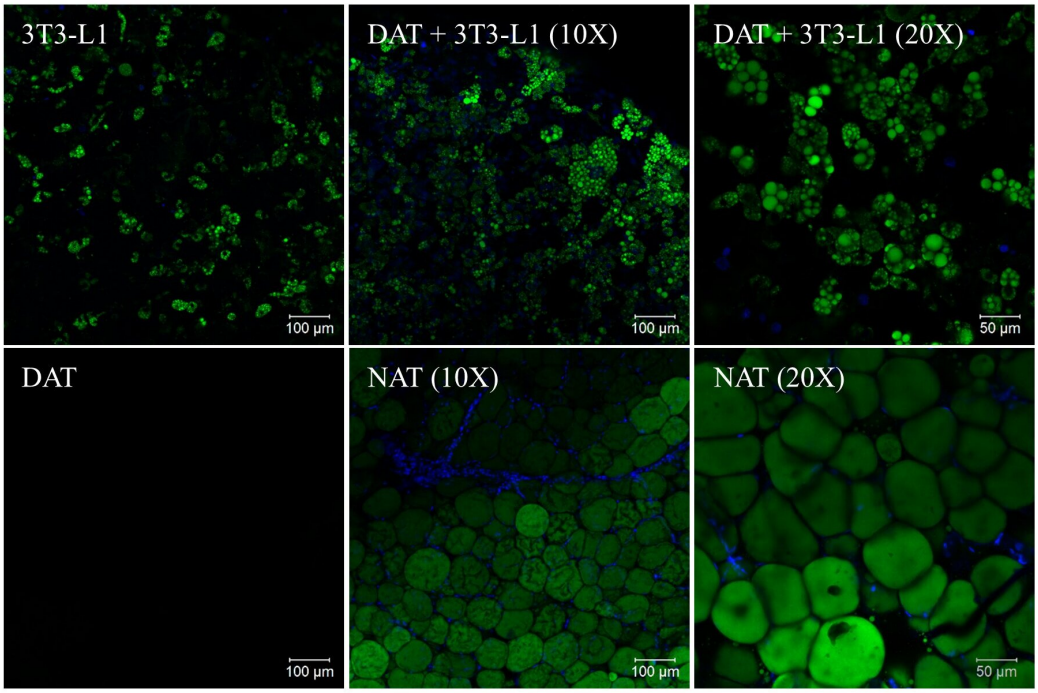

Fig. 7. Stained lipid droplets in NAT, DAT, DAT + 3T3-L1 and 3T3-L1 on cell culture plastic. 3T3-L1 cells grown in DAT for 28 days compared to a 3T3-L1 only, DAT only and NAT stained with BODIPY 493/503 (green) and DAPI (blue). Scale bars represent 100 μm. Lipid droplets appear green, and nuclei appear blue.

this decellularisation protocol was more effective at preserving the ECM whilst removing cellular material.

A 40% reduction in the diameter of the basement membrane from around adipocytes was observed, highlighting the collapse of the basement membrane. The removal of the cells will have caused a reduction in pressure placed on the basement membrane by the cell traction forces from adipocytes. Cell traction forces have been correlated with adipocyte cell area and cytoskeletal-focal adhesion architecture development, which are responsible for cell-to-ECM force transmission [50]. Therefore, the reduction of this force transmission due to the loss of adipocytes is the likely cause of the basement membrane collapse. In the literature, cell migration, proliferation and differentiation have been shown to be influenced by cell traction forces, suggesting that this may impede host cell infiltration into DAT once implanted [51]. Although there was a shrinkage of the basement membrane in DAT, this did not discourage cell infiltration into the DAT. The data also suggest that DAT was able to support the growth of both 3T3 and 3T3-L1 cells, which maintained cell viability; however, the metabolic activity was lower in cells grown in DAT than that of the cell-only controls. Previous studies have noted that 3D culture can affect cell metabolic activity and reduce cell proliferation, which is thought to occur due to limited oxygen and nutrient penetration [52,53]. However, Rybkowska *et al.* [52] (2023) used more specific measures of metabolic activity than in the current study, such as oxygen consumption rate and extracellular acidification rate. Though these should correlate with alamarBlue™ conversion, there are other aspects involved with alamarBlue™ that could account for the reduced reduction of alamarBlue™ with seeded DAT compared to cell-only controls, such as dye becoming trapped in the DAT.

The potential of 3T3-L1 cells seeded onto the DAT to differentiate into adipocyte-like cells was measured by investigating lipid accumulation. After 28 days of culture, 3T3-L1 cells seeded on DAT in the absence of adipogenic differentiation factors showed evidence of lipid accumulation, and a similar effect was seen when the cells were grown on tissue culture plastic. It has previously been reported that 3T3-L1 cells can accumulate lipids in the absence of adipogenic differentiation media when they reach sufficient confluency to elicit growth arrest [54]. While this could explain the lipid accumulation observed in the 2D tissue culture plastic control, the cells on the DAT scaffold were not fully confluent due to the large surface area of the DAT. Therefore, the lipid accumulation in 3T3-L1 cells in DAT may have been due to a response to the DAT topography or microenvironmental cues received upon adhesion to the ECM [53]. However, as the 3T3-L1 cells began to

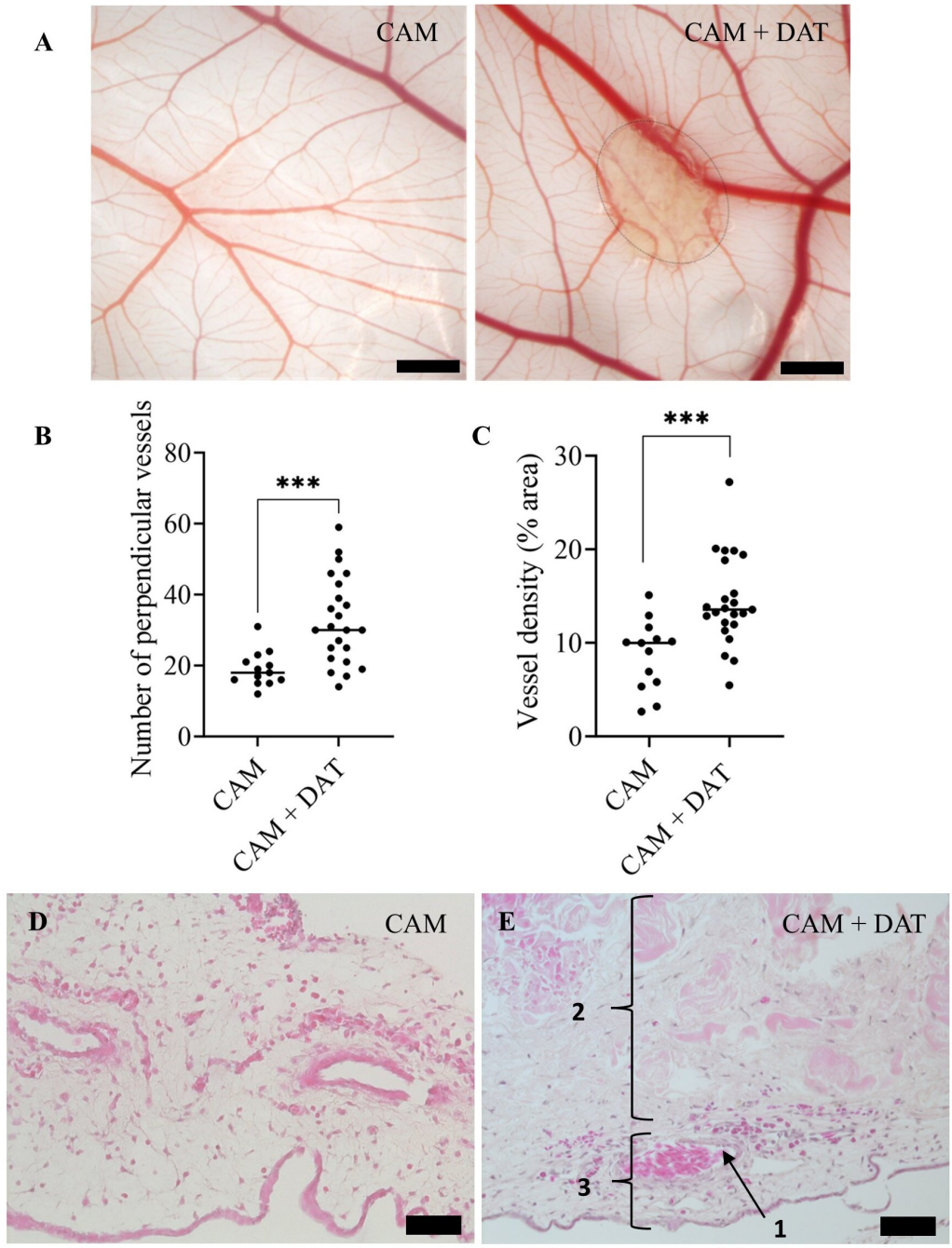

Fig. 8. Vascular growth towards DAT within a CAM model. Representative images of the DAT placed on the CAM (DAT circled in images) (**A**) Scale bars = 2 mm. ImageJ analysis of panel A, highlighting directional vessel growth at 90° ± 45° (**B**) and vessel density (**C**) Graphs show the median and distribution of the dataset ***$p < 0.001$ confirmed using a two-tailed Welch's test following normality confirmation with a Shapiro-Wilk test. Vessel density was transformed using arcsine function prior to statistical analysis. Representative histological images of CAM and DAT cross sections stained with H&E (**D** & **E**) Scale bars = 50 μm. Annotations: 1 = blood vessels containing red blood cells, 2 = DAT, 3 = CAM. (n = 6 (DAT), n = 5 (CAM per DAT)).

differentiate into adipocytes within the DAT, this would reduce their proliferative ability. Therefore, it could account for a reduction in metabolic activity, as the metabolic activity of terminally differentiated mature adipocytes would be decreased.

The BODIPY 493/503 results suggest that DAT provided an inductive microenvironment for adipocyte differentiation, as has been shown previously with human-

derived DAT and ECM [19,55]. However, these papers used ADSCs rather than 3T3-L1 cells to assess human-based DAT *in vitro*. Proteins, growth factors and extracellular vesicles bound to ECM molecules have been shown to remain following decellularisation to provide tissue-specific signalling in several different tissues, including small intestinal submucosa [56,57]. Further investigation is required to determine which of these factors remain on the DAT produced in this study and whether these provide adipogenic signals for adipocyte growth and differentiation. The lipid droplets in 3T3-L1 cells grown in DAT were smaller than NAT, as commonly seen with 3T3-L1 cells in culture [58,59]. It was also observed that the 3T3-L1 cells do not acquire the unilocular phenotype of mature native adipocytes; however, this has been reported elsewhere regarding primary and cell line-derived preadipocytes and has been attributed to adipocyte immaturity [58–61]. Longer-term culture and the addition of differentiation factors may provide more information on this behaviour. In the literature, the growth of adipocytes with unilocular lipid droplets is considered difficult in culture, as they are believed to have reached a terminal differentiation, so they will no longer continue to proliferate [62]. Recently, it has been discovered that aerobic glycolysis in 3D adipocyte culture increases AMP-activated protein kinase activation, leading to increased fatty acid uptake and the formation of unilocular lipids. Therefore, the experiment could be repeated with ADSCs and upregulated aerobic glycolysis to understand whether DAT is able to support unilocular lipid development [63]. Alternatively, the formation of unilocular lipids within adipocytes should be assessed during *in vivo* studies.

The CAM assay was used as a method of studying cellular response to DAT in a more complex model. The survival rate of the eggs was 66% after removal from the shell, which is greater than previously reported (50–60%) when using the *ex ovo* method [64]. Both an increase in vessel density and directional vessel growth toward the DAT occurred within the CAM sample, which suggests that DAT may be able to support the growth of new vessels. Angiogenesis is a key aspect in the wound healing process; therefore, the growth of new vessels is of key importance. The infiltration of cells from the CAM into DAT, seen in the histological analysis, corroborates the *in vitro* results demonstrating DAT's capacity to support cell migration and infiltration. Similar histological data have been shown with Alloderm, a clinically used acellular human dermis produced by LifeCell, which displayed successful cell infiltration into the implanted Alloderm within *in vivo* mouse studies [65,66]. Though this does not directly relate to adipose regeneration, this is an example of a decellularised graft with clinical success in a similar area to adipose regeneration. Based on the results of this study, it is expected that DAT has the potential to integrate after implantation.

The potential applications for DAT are broad, including the regeneration of adipose tissues for patients who have had a mastectomy, adipose volume loss following traumatic injuries or patients with diabetic foot ulcers. Though there are benefits to the use of porcine tissue, including wider availability and lower costs, DAT has been developed mostly from human sources [9,19]. Therefore, in the future, we could adapt this protocol to decellularise human adipose tissue.

Conclusions

In conclusion, this study has successfully produced porcine-derived DAT sheets, which preserved the ECM and met the criteria for successful decellularisation. *In vitro* assessment has shown that DAT is non-cytotoxic to L929 and 3T3 cells. DAT supports 3T3 and 3T3-L1 cell adhesion, cell viability and supports the differentiation of 3T3-L1 cells to adipocyte-like cells in the absence of adipogenic differentiation factors. Additionally, blood vessels grew towards DAT within the CAM *ex ovo* assay. These factors suggest that DAT is likely to be integrated *in vivo*; however, future research will further investigate the biochemical behaviour of DAT and its potential as a treatment for adipose regeneration.

Abbreviations

DAT, decellularised adipose tissue; ADSCs, Adipose derived stromal cells; ECM, extracellular matrix; ds-DNA, double stranded DNA; CAM, chick chorioallantoic membrane; SDS, Sodium dodecyl sulphate; IPA, isopropanol; PBS, phosphate buffered saline; NAT, native adipose tissue; DMEM, Dulbecco's Modified Eagles Medium; FBS, foetal bovine serum; NBF, neutral buffered formalin; H&E, Haematoxylin and eosin; UKHSA, UK Health Security Agency; DMSO, Dimethylsulphoxide; EDTA, Ethylenediaminetetraacetic acid; DAPI, 4′,6-diamidino-2-phenylindole.

Availability of Data and Materials

All raw data files have been deposited into the Research Data Leeds repository. Access is available through https://doi.org/10.5518/1645.

Author Contributions

J.H.E. was responsible for the initial scientific concept for creating DAT. All authors (L.M.O., R.F., V.L.W., C.L.R., J.H.E., V.L.H., and H.E.B.) contributed to study design and development. Material preparation, data collection, and analysis were performed by L.M.O. Author R.F. facilitated the study design and analysis of the CAM assays and undertook set up and data collection within this. The first draft of the manuscript was written by L.M.O. All authors (as above) commented on previous versions of the manuscript and read and approved the final manuscript. All authors agree to be accountable for all aspects of the work in

ensuring that questions related to the accuracy or integrity of any part of the work are appropriately investigated and resolved.

Ethics Approval and Consent to Participate

Ethical approval for the use of porcine tissue within this study was not required as the animal tissue was sourced from the UK food chain. The use of animal embryos was conducted under the approval of the University of Leeds Animal Welfare Ethical Review Committee as non-regulated animal work. As the embryos were sacrificed before 14 days of incubation, these did not fall under the Animals in Scientific Procedures Act (2012). However, care was taken to reduce tissue wastage, treat animal tissue respectfully and to use appropriate storage and disposal of tissues.

Acknowledgments

The Authors would like to acknowledge the help of Dr Sally Boxall and Dr Ruth Hughes for the use and support with Confocal Microscopy within the Bioimaging Facility, at the University of Leeds.

Funding

This work was funded by the Faculty of Biological Sciences at the University of Leeds, as received by J.H Edwards.

Conflict of Interest

There are no relevant financial or non-financial interests to disclose by any of the authors.

References

[1] Dragoo JL, Shapiro SA, Bradsell H, Frank RM. The essential roles of human adipose tissue: Metabolic, thermoregulatory, cellular, and paracrine effects. Journal of Cartilage & Joint Preservation. 2021; 1: 100023. https://doi.org/10.1016/j.jcjp.2021.100023.

[2] Shook BA, Wasko RR, Mano O, Rutenberg-Schoenberg M, Rudolph MC, Zirak B, *et al*. Dermal Adipocyte Lipolysis and Myofibroblast Conversion Are Required for Efficient Skin Repair. Cell Stem Cell. 2020; 26: 880–895.e6. https://doi.org/10.1016/j.stem.2020.03.013.

[3] Zhao H, Shang Q, Pan Z, Bai Y, Li Z, Zhang H, *et al*. Exosomes From Adipose-Derived Stem Cells Attenuate Adipose Inflammation and Obesity Through Polarizing M2 Macrophages and Beiging in White Adipose Tissue. Diabetes. 2018; 67: 235–247. https://doi.org/10.2337/db17-0356.

[4] Wu Z, Wang Z, Chen T, Wang D, Zhou F, Zhang G, *et al*. Dermal white adipose tissue: A new modulator in wound healing and regeneration. Regenerative Therapy. 2025; 28: 115–125. https://doi.org/10.1016/j.reth.2024.11.015.

[5] Alkhouli N, Mansfield J, Green E, Bell J, Knight B, Liversedge N, *et al*. The mechanical properties of human adipose tissues and their relationships to the structure and composition of the extracellular matrix. American Journal of Physiology-Endocrinology and Metabolism. 2013; 305: E1427–E1435. https://doi.org/10.1152/ajpendo.00111.2013.

[6] Mahoney CM, Imbarlina C, Yates CC, Marra KG. Current Therapeutic Strategies for Adipose Tissue Defects/Repair Using Engineered Biomaterials and Biomolecule Formulations. Frontiers in Pharmacology. 2018; 9: 507. https://doi.org/10.3389/fphar.2018.00507.

[7] Shih L, Davis MJ, Winocour SJ. The Science of Fat Grafting. Seminars in Plastic Surgery. 2020; 34: 5–10. https://doi.org/10.1055/s-0039-3402073.

[8] Simonacci F, Bertozzi N, Grieco MP, Grignaffini E, Raposio E. Procedure, applications, and outcomes of autologous fat grafting. Annals of Medicine and Surgery. 2017; 20: 49–60. https://doi.org/10.1016/j.amsu.2017.06.059.

[9] Kokai LE, Schilling BK, Chnari E, Huang YC, Imming EA, Karunamurthy A, *et al*. Injectable Allograft Adipose Matrix Supports Adipogenic Tissue Remodeling in the Nude Mouse and Human. Plastic and Reconstructive Surgery. 2019; 143: 299e–309e. https://doi.org/10.1097/PRS.0000000000005269.

[10] Qin Y, Ge G, Yang P, Wang L, Qiao Y, Pan G, *et al*. An Update on Adipose-Derived Stem Cells for Regenerative Medicine: Where Challenge Meets Opportunity. Advanced Science. 2023; 10: 2207334. https://doi.org/10.1002/advs.202207334.

[11] Zhang J, Wu K, Zhou L, Zheng S. Adipose-Derived Stem Cells for Cartilage Tissue Engineering: A Bibliometric Analysis of Trends and Themes. Journal of Multidisciplinary Healthcare. 2025; 18: 3023–3037. https://doi.org/10.2147/jmdh.S522203.

[12] Palpant NJ, Metzger JM. Aesthetic cardiology: adipose-derived stem cells for myocardial repair. Current Stem Cell Research & Therapy. 2010; 5: 145–152. https://doi.org/10.2174/157488810791268654.

[13] Casadei A, Epis R, Ferroni L, Tocco I, Gardin C, Bressan E, *et al*. Adipose tissue regeneration: a state of the art. Journal of Biomedicine and Biotechnology. 2012; 2012: 462543. https://doi.org/10.1155/2012/462543.

[14] Liang R, Pan R, He L, Dai Y, Jiang Y, He S, *et al*. Decellularized Extracellular Matrices for Skin Wound Treatment. Materials (Basel). 2025; 18: 2752. https://doi.org/10.3390/ma18122752.

[15] Waqanivavalagi SWFR, Bhat S, Ground MB, Milsom PF, Cornish J. Clinical performance of decellularized heart valves versus standard tissue conduits: a systematic review and meta-analysis. Journal of Cardiothoracic Surgery. 2020; 15: 260. https://doi.org/10.1186/s13019-020-01292-y.

[16] Nakamura N, Kimura T, Kishida A. Overview of the Development, Applications, and Future Perspectives of Decellularized Tissues and Organs. ACS Biomaterials Science & Engineering. 2017; 3: 1236–1244. https://doi.org/10.1021/acsbiomaterials.6b00506.

[17] Duong VT, Nguyen HD, Luong NH, Chang CY, Lin CC. Photo-Responsive Decellularized Small Intestine Submucosa Hydrogels. Advanced Functional Materials. 2024; 34: 2401952. https://doi.org/10.1002/adfm.202401952.

[18] Solarte David VA, Güiza-Argüello VR, Arango-Rodríguez ML, Sossa CL, Becerra-Bayona SM. Decellularized Tissues for Wound Healing: Towards Closing the Gap Between Scaffold Design and Effective Extracellular Matrix Remodeling. Frontiers in bioengineering and biotechnology. 2022; 10: 821852. https://doi.org/10.3389/fbioe.2022.821852.

[19] Flynn LE. The use of decellularized adipose tissue to provide an inductive microenvironment for the adipogenic differentiation of human adipose-derived stem cells. Biomaterials. 2010; 31: 4715–4724. https://doi.org/10.1016/j.biomaterials.2010.02.046.

[20] Bi X, Li Y, Dong Z, Zhao J, Wu W, Zou J, *et al*. Recent Developments in Extracellular Matrix Remodeling for Fat Grafting. Frontiers in Cell and Developmental Biology. 2021; 9: 767362. https://doi.org/10.3389/fcell.2021.767362.

[21] Laude M, Kolliopoulos V, Mikos AG, White LJ, Cosgriff-Hernandez E. Extracellular-Matrix-Based Materials from Decellularized Tissue: Opportunities, Challenges, and Future Directions in Regenerative Medicine. Advanced Healthcare Materials. 2026; 15: e02107. https://doi.org/10.1002/adhm.202502107.

[22] Diller RB, Tabor AJ. The Role of the Extracellular Matrix (ECM) in Wound Healing: A Review. Biomimetics. 2022; 7: 87. https://doi.org/10.3390/biomimetics7030087.

[23] Midwood KS, Williams LV, Schwarzbauer JE. Tissue repair and the dynamics of the extracellular matrix. The International Journal of Biochemistry & Cell Biology. 2004; 36: 1031–1037. https://doi.org/10.1016/j.biocel.2003.12.003.

[24] Mughal M, Sindali K, Man J, Roblin P. 'Fat chance': a review of adipose tissue engineering and its role in plastic and reconstructive surgery. Annals of the Royal College of Surgeons of England. 2021; 103: 245–249. https://doi.org/10.1308/rcsann.2020.7031.

[25] Banyard DA, Borad V, Amezcua E, Wirth GA, Evans GR, Widgerow AD. Preparation, Characterization, and Clinical Implications of Human Decellularized Adipose Tissue Extracellular Matrix (hDAM): A Comprehensive Review. Aesthetic Surgery Journal. 2016; 36: 349–357. https://doi.org/10.1093/asj/sjv170.

[26] Choi YC, Choi JS, Kim BS, Kim JD, Yoon HI, Cho YW. Decellularized Extracellular Matrix Derived from Porcine Adipose Tissue as a Xenogeneic Biomaterial for Tissue Engineering. Tissue Engineering Part C: Methods. 2012; 18: 866–876. https://doi.org/10.1089/ten.tec.2012.0009.

[27] Wang L, Johnson JA, Zhang Q, Beahm EK. Combining decellularized human adipose tissue extracellular matrix and adipose-derived stem cells for adipose tissue engineering. Acta Biomaterialia. 2013; 9: 8921–8931. https://doi.org/10.1016/j.actbio.2013.06.035.

[28] Sesli M, Akbay E, Onur MA. Decellularization of rat adipose tissue, diaphragm, and heart: a comparison of two decellularization methods. Turkish Journal of Biology. 2018; 42: 537–547. https://doi.org/10.3906/biy-1807-109.

[29] Xia Z, Guo X, Yu N, Zeng A, Si L, Long F, *et al*. The Application of Decellularized Adipose Tissue Promotes Wound Healing. Tissue Engineering and Regenerative Medicine. 2020; 17: 863–874. https://doi.org/10.1007/s13770-020-00286-0.

[30] Anderson AE, Wu I, Parrillo AJ, Wolf MT, Maestas DR, Graham I, *et al*. An immunologically active, adipose-derived extracellular matrix biomaterial for soft tissue reconstruction: concept to clinical trial. NPJ Regenerative medicine. 2022; 7: 6. https://doi.org/10.1038/s41536-021-00197-1.

[31] Neishabouri A, Soltani Khaboushan A, Daghigh F, Kajbafzadeh AM, Majidi Zolbin M. Decellularization in Tissue Engineering and Regenerative Medicine: Evaluation, Modification, and Application Methods. Frontiers in Bioengineering and Biotechnology. 2022; 10: 805299. https://doi.org/10.3389/fbioe.2022.805299.

[32] Mendibil U, Ruiz-Hernandez R, Retegi-Carrion S, Garcia-Urquia N, Olalde-Graells B, Abarrategi A. Tissue-Specific Decellularization Methods: Rationale and Strategies to Achieve Regenerative Compounds. International Journal of Molecular Science. 2020; 21: 5447. https://doi.org/10.3390/ijms21155447.

[33] Liu J, Song Q, Yin W, Li C, An N, Le Y, *et al*. Bioactive scaffolds for tissue engineering: A review of decellularized extracellular matrix applications and innovations. Exploration. 2024; 5: 20230078. https://doi.org/10.1002/EXP.20230078.

[34] Lin YC, Grahovac T, Oh SJ, Ieraci M, Rubin JP, Marra KG. Evaluation of a multi-layer adipose-derived stem cell sheet in a full-thickness wound healing model. Acta Biomaterialia. 2013; 9: 5243–5250. https://doi.org/10.1016/j.actbio.2012.09.028.

[35] Patel NG, Zhang G. Stacked stem cell sheets enhance cell-matrix interactions. Organogenesis. 2014; 10: 170–176. https://doi.org/10.4161/org.28990.

[36] Crapo PM, Gilbert TW, Badylak SF. An overview of tissue and whole organ decellularization processes. Biomaterials. 2011; 32: 3233–3243. https://doi.org/10.1016/j.biomaterials.2011.01.057.

[37] Gratzer PF, Harrison RD, Woods T. Matrix Alteration and Not Residual Sodium Dodecyl Sulfate Cytotoxicity Affects the Cellular Repopulation of a Decellularized Matrix. Tissue Engineering. 2006; 12: 2975–2983. https://doi.org/10.1089/ten.2006.12.2975.

[38] Mitoulas LR, Kent JC, Cox DB, Owens RA, Sherriff JL, Hartmann PE. Variation in fat, lactose and protein in human milk over 24h and throughout the first year of lactation. The British journal of nutrition. 2002; 88: 29–37. https://doi.org/10.1079/BJN2002579.

[39] Samourides A, Browning L, Hearnden V, Chen B. The effect of porous structure on the cell proliferation, tissue ingrowth and angiogenic properties of poly(glycerol sebacate urethane) scaffolds. Materials Science and Engineering: C. 2020; 108: 110384. https://doi.org/10.1016/j.msec.2019.110384.

[40] Muchová J, Hearnden V, Michlovská L, Vištejnová L, Zavaďáková A, Šmerková K, *et al*. Mutual influence of selenium nanoparticles and FGF2-STAB® on biocompatible properties of collagen/chitosan 3D scaffolds: in vitro and ex ovo evaluation. Journal of Nanobiotechnology. 2021; 19: 103. https://doi.org/10.1186/s12951-021-00849-w.

[41] Schindelin J, Arganda-Carreras I, Frise E, Kaynig V, Longair M, Pietzsch T, *et al*. Fiji: an open-source platform for biological-image analysis. Nature Methods. 2012; 9: 676–682. https://doi.org/10.1038/nmeth.2019.

[42] Elfarnawany MH. Signal Processing Methods for Quantitative Power Doppler Microvascular Angiography [PhD thesis]. Canada: Western University. 2015.

[43] Pritt B, Tessitore JJ, Weaver DL, Blaszyk H. The effect of tissue fixation and processing on breast cancer size. Human Pathology. 2005; 36: 756–760. https://doi.org/10.1016/j.humpath.2005.04.018.

[44] Cartmell JS, Dunn MG. Development of Cell-Seeded Patellar Tendon Allografts for Anterior Cruciate Ligament Reconstruction. Tissue Engineering. 2004; 10: 1065–1075. https://doi.org/10.1089/ten.2004.10.1065.

[45] Young DA, Ibrahim DO, Hu D, Christman KL. Injectable hydrogel scaffold from decellularized human lipoaspirate. Acta Biomaterialia. 2011; 7: 1040–1049. https://doi.org/10.1016/j.actbio.2010.09.035.

[46] Kaufman MR, Miller TA, Huang C, Roostaien J, Wasson KL, Ashley RK, *et al*. Autologous Fat Transfer for Facial Recontouring: Is There Science behind the Art? Plastic and Reconstructive Surgery. 2007; 119: 2287–2296. https://doi.org/10.1097/01.prs.0000260712.44089.e7.

[47] Cuono C, Langdon R, McGuire J. Use of cultured epidermal autografts and dermal allografts as skin replacement after burn injury. Lancet. 1986; 1: 1123–1124. https://doi.org/10.1016/s0140-6736(86)91838-6.

[48] Voytik-Harbin SL, Brightman AO, Waisner BZ, Robinson JP, Lamar CH. Small Intestinal Submucosa: A Tissue-Derived Extracellular Matrix That Promotes Tissue-Specific Growth and Differentiation of Cells in Vitro. Tissue Engineering. 1998; 4: 157–174. https://doi.org/10.1089/ten.1998.4.157.

[49] Kim BS, Choi JS, Kim JD, Choi YC, Cho YW. Recellularization of decellularized human adipose-tissue-derived extracellular matrix sheets with other human cell types. Cell and Tissue Research. 2012; 348: 559–567. https://doi.org/10.1007/s00441-012-1391-y.

[50] Bouzid T, Esfahani AM, Safa BT, Kim E, Saraswathi V, Kim JK, *et al*. Rho/ROCK mechanosensor in adipocyte stiffness and traction force generation. Biochemical and Biophysical Research Communications. 2022; 606: 42–48. https://doi.org/10.1016/j.bbrc.2022.03.078.

[51] Zhang M, Zhang Y, Wang P, Sun Q, Wang X, Cao Y, *et al*. A detailed protocol for cell force measurement by traction force microscopy. Smart Materials in Medicine. 2024; 5: 106–113. https://doi.org/10.1016/j.smaim.2023.08.002.

[52] Rybkowska P, Radoszkiewicz K, Kawalec M, Dymkowska D, Zabłocka B, Zabłocki K, *et al*. The Metabolic Changes between Monolayer (2D) and Three-Dimensional (3D) Culture Conditions in Human Mesenchymal Stem/Stromal Cells Derived from Adipose Tissue. Cells. 2023; 12: 178. https://doi.org/10.3390/cells12010178.

[53] Baker BM, Chen CS. Deconstructing the third dimension – how 3D culture microenvironments alter cellular cues. Journal of Cell Sci-

ence. 2012; 125: 3015–3024. https://doi.org/10.1242/jcs.079509.
[54] Green H, Kehinde O. Sublines of mouse 3T3 cells that accumulate lipid. Cell. 1974; 1: 113–116. https://doi.org/10.1016/0092-8674(74)90126-3.
[55] Qian Y, Chen H, Pan T, Li T, Zhang Z, Lv X, *et al*. Autologous decellularized extracellular matrix promotes adipogenic differentiation of adipose derived stem cells in low serum culture system by regulating the ERK1/2-PPARγ pathway. Adipocyte. 2021; 10: 174–188. https://doi.org/10.1080/21623945.2021.1906509.
[56] Hodde JP, Record RD, Liang HA, Badylak SF. Vascular Endothelial Growth Factor in Porcine-Derived Extracellular Matrix. Endothelium. 2001; 8: 11–24. https://doi.org/10.3109/10623320109063154.
[57] Cramer MC, Badylak SF. Extracellular Matrix-Based Biomaterials and Their Influence Upon Cell Behavior. Annals of Biomedical Engineering. 2020; 48: 2132–2153. https://doi.org/10.1007/s10439-019-02408-9.
[58] Rizzatti V, Boschi F, Pedrotti M, Zoico E, Sbarbati A, Zamboni M. Lipid droplets characterization in adipocyte differentiated 3T3-L1 cells: size and optical density distribution. European Journal of Histochemistry. 2013; 57: e24. https://doi.org/10.4081/ejh.2013.e24.
[59] Josan C, Kakar S, Raha S. Matrigel® enhances 3T3-L1 cell differentiation. Adipocyte. 2021; 10: 361–377. https://doi.org/10.1080/21623945.2021.1951985.
[60] Sugihara H, Yonemitsu N, Toda S, Miyabara S, Funatsumaru S, Matsumoto T. Unilocular fat cells in three-dimensional collagen gel matrix culture. Journal of Lipid Research. 1988; 29: 691–697. https://doi.org/10.1016/S0022-2275(20)38514-X.
[61] Dufau J, Shen JX, Couchet M, De Castro Barbosa T, Mejhert N, Massier L, *et al*. In vitro and ex vivo models of adipocytes. American Journal of Physiology-Cell Physiology. 2021; 320: C822–C841. https://doi.org/10.1152/ajpcell.00519.2020.
[62] Sugihara H, Yonemitsu N, Miyabara S, Toda S. Proliferation of unilocular fat cells in the primary culture. Journal of Lipid Research. 1987; 28: 1038–1045. https://doi.org/10.1016/S0022-2275(20)38619-3.
[63] Maestri A, Cai M, Schipper R, Backman J, Vannay A, Olsson A, *et al*. Aerobic glycolysis drives differentiation of unilocular adipocytes. Journal of Lipid Research. 2026; 67: 101023. https://doi.org/10.1016/j.jlr.2026.101023.
[64] Naik M, Brahma P, Dixit M. A Cost-Effective and Efficient Chick Ex-Ovo CAM Assay Protocol to Assess Angiogenesis. Methods and Protocols. 2018; 1: 19. https://doi.org/10.3390/mps1020019.
[65] Kulig KM, Luo X, Finkelstein EB, Liu XH, Goldman SM, Sundback CA, *et al*. Biologic properties of surgical scaffold materials derived from dermal ECM. Biomaterials. 2013; 34: 5776–5784. https://doi.org/10.1016/j.biomaterials.2013.02.055.
[66] Chien PN, Zhang XR, Nilsu D, Faruq O, VAN Anh LT, Nam SY, *et al*. In Vivo Comparison of Three Human Acellular Dermal Matrices for Breast Reconstruction. In Vivo. 2021; 35: 2719–2728. https://doi.org/10.21873/invivo.12556.

Editor's note: The Scientific Editors responsible for this paper were Moroni Lorenzo and Martin Stoddart.

Received: 5th December 2025; **Accepted**: 10th August 2026; **Published**: 30th September 2026